

Novel Adaptive Impedance Control for Exoskeleton Robot for Rehabilitation Using a Nonlinear Time-Delay Disturbance Observer

Brahim Brahmi, Mark Driscoll, Ibrahim K. El Bojairami
Musculoskeletal Biomechanics Research Lab
Mechanical Engineering Department | McGill University,
Montreal, Canada

brahim.brahmi@mcgill.ca, mark.driscoll@mcgill.ca, ibrahim.elbojairami@mail.mcgill.ca

Maarouf Saad, Abdelkrim Brahmi
Electrical Engineering Department
École de Technologie supérieure
Montreal, Canada
maarouf.saad@etsmtl.ca, abdelkrim.brahmi.1@ens.etsmtl.ca

Abstract: A new adaptive impedance, augmented with backstepping, control, combined with time-delay estimation, and a disturbance observer was designed to perform passive-assistive rehabilitation motion. This was done using a rehabilitation robot whereby humans' musculoskeletal conditions were considered. This control scheme aims to mimic the movement behavior of the user and to provide an accurate compensation of uncertainties and torque disturbances. Such disturbances were excited by constraints of input saturation of the robot's actuators, friction forces and backlash, several payloads of the attached upper-limb of each patient, and time delay errors. The designed impedance control algorithm would transfer the stiffness of the human upper limb to the developed impedance model via the measured user force. In the proposed control scheme, active rejection of disturbances would be achieved by the direct connection of such disturbances from the observer's output with the control input via the feedforward loop of the system. Furthermore, the computed control input does not require any precise knowledge of the robot's dynamic model or any knowledge of built-in torque-sensing units to provide the desirable physiotherapy treatment. Experimental investigations performed by two subjects were exhibited to support the benefits of the designed approach.

Index Terms—Rehabilitation robot, Impedance control, approximation-based control, time-delay estimation (TDE), disturbances observer.

I. INTRODUCTION

Recently, the implementation of exoskeleton robots in the rehabilitation medical field has proven to reduce musculoskeletal impairments, enhancing patients' range of motion and enabling them to perform more frequent activities [1-4]. Due to the complex mechanical configuration of the humans exoskeleton robots, and the high sensitivity of the human-robot interaction, maneuvering such robots presents additional intricacy compared to controlling conventional manipulators [5, 6]. For instance, an indirect force-control based on Electromyography (EMG) signals [7] allows the subject to maneuver an exoskeleton robot to accomplish the desired physiotherapy exercise. Further, on the other hand, dynamic model-based control has been applied to an exoskeleton robot through a computed torque controller [8]. To resolve such issues, a sliding-mode controller, integrated with an exponential reaching law, has been used [9]. Clearly, the referenced investigations used model-based control strategies, for which the exoskeleton dynamic model should be explicitly formulated.

Security and comfort during human use are critical criteria to consider upon the interaction with the exoskeleton robot during rehabilitation sessions. To achieve this, the control system requires manifold measured data from the exoskeleton robot, such as joint torques. Joint torques based control strategies have been widely implemented to maintain safety of rehabilitation robots. Such proposals included a built-in torque measuring strategy based on an estimated gain [10] and a joint torques sensors-based

measurements strategy [11] for lightweight exoskeleton robots. Besides their complicated features, these approaches suffer from the imprecise calibration and thus errors spanning from joint torque sensors. On the other hand, disturbance observers based approaches are also abundant [12-16]. The primary role of the disturbance observer is to consider all unknown uncertainties and disturbances, whether internal or external, as an unknown function in order to approximate them. The compensation of this unknown function is obtained directly by combining disturbance observer's output with the control input. In this case, rapid, high-quality tracking performance and smooth control inputs can be achieved without choosing significant feedback gains due to the nature of this type of feedforward compensation.

The estimation of the dynamic parameters of exoskeleton robots is one of the common challenging endeavors in robotic rehabilitation systems, particularly if the exoskeleton robot has a high degree of freedom (DOF). In fact, the stiffness and varying musculoskeletal models of the human upper limb during motion can also affect the robustness of the control system. As such, the adaptation of the human upper limb behavior plays a significant role in providing suitable rehabilitation treatment. Approximation-based control methods, such as linearization of the dynamic model, were previously employed to estimate the unknown dynamic parameters of the robot [17-19]. Mostly, these methods utilize the linear parameterization properties of the robot's dynamic model to obtain the associated regressor matrix, which the control law is commonly based on. Nonetheless, these approaches suffer from two major problems. Firstly, it is arduous to get the robot dynamic parameters when the system has high number of DOFs. For example, the dynamic parameters' vector of the exoskeleton can exceed one hundred if the DOFs of the exoskeleton is more than four [20]. Secondly, the integral action of the updated law might produce instabilities, even under small disturbances. On the other hand, fuzzy logic and neural network are recently widely used in efforts of approximating the unknown dynamic parameters of rehabilitation robots [21-23]. Yet, such methods are influenced by the size of the input-output variables of the system, in addition to the approximation rules that makes the convergence of the estimated weight to its actual state during the operation of weight training becoming time-consuming. Such limitations make the real-time application of rehabilitation robots challenging.

To resolve the aforementioned limitations, Time Delay Estimation (TDE) [24, 25] presents itself as a plausible solution. Due to the fact that it has shown distinct performance when implemented in numerous physical systems [26, 27], it has been decided to employ it in the present paper to approximate the unknown values of the exoskeleton dynamic model. Another factor behind the selection of TDE is due to its ease of implementation in real-time applications. Besides, TDE is one of the approaches that are not influenced by the dimension of the input-output of dynamic systems in the case of high DOFs. It is sufficient to delay the input-output of the system by only one step to estimate the unknown dynamical system. Nonetheless, the Time Delay Error (TDR) remains a challenge when using TDE strategy. This error is generated by loud nonlinearity of the unknown dynamical system during the delay constant, which would diminish the estimation's precision. Accordingly, the purpose of the present research is to incorporate Time Delay Estimation with disturbance observer to estimate the unknown functions as well as compensating for the TDR, constraints of input saturation, and unexpected disturbances. Furthermore, such advantages of incorporating the Time Delay Estimation with the disturbance observer for exoskeleton robots are exploited to analyze the performance achieved by this theoretical and practical system integration.

In addition, input saturation constraint is one of the nonlinear components that can decrease robot's performances. Consequently, the performance of the exoskeleton robot would decrease where the control system becomes incapable of producing the required effort to permit human-exoskeleton robots to achieve desired physical therapy movements. Eliminating this constraint makes the rehabilitation robot system dangerous to the exoskeleton's user. As such, many techniques are proposed to overcome the limitations of the input saturation, such as the saturated PID controller for industrial robots [28], and nonlinear disturbance observers based on fuzzy logic and neural network intelligent control systems [29, 30]. As previously mentioned, such techniques require computationally expensive in real time, making their implementation questionable. This motivates researchers to design exoskeleton robot controllers able to reduce the influence of the actuators saturation constraints and ensure system's stability.

Motivated by the aforementioned problems related to uncertainty dynamics caused by constraints of robots actuators input saturation, Time Delay Errors (TDR), friction forces, patients' physiological variabilities including mass of the upper-limb, and previous work [31, 32], an adaptive impedance control augmented with backstepping controller has been implemented for wearable exoskeleton robots with unknown uncertainty dynamics using the user's force feedback. This was achieved by developing an in-silico human musculoskeletal model to match user's motion behavior. That is, the proposed impedance control was designed to transfer the stiffness of the human upper limb to the impedance model scheme. This permits to compensate for human muscles activity (considered as un-matched disturbances) during rehabilitation tasks directly via regulator variables of the backstepping controller. Backstepping control allows only for the compensation of uncertainties solely decreasing together with the state variables, which are matched disturbances. Following this, a combined disturbance approximation based on Time Delay Estimation (TDE) was developed, for which the disturbance variable constituted of joint couplings, variable masses, and nonlinear dynamic uncertainty. Sources of torque perturbation can potentially be the constraints of saturation, Time Delay Errors (TDR), friction forces, and payload. The disturbance observer output, directly connected to the proposed control scheme via a feedforward loop, allows the control algorithm to be robust and productive to reduce the impact of disturbances. The integration of an adaptive impedance model, backstepping controller, TDE, all together with a disturbance observer, generates a robust control scheme. This would eliminate matched and unmatched disturbances in the absence of the entire exoskeleton dynamic model. The proposed control scheme was lastly validated against a real test subject using fundamental passive rehabilitation therapy. A comparative study with conventional approaches highlighted the superior performance of the proposed control scheme in real time - a key requirement of rehabilitation robots. The contributions can be summarized as follows:

- 1) A human musculoskeletal model of the upper limb was designed to match user's kinematic and dynamic behavior directly via regular variables of backstepping controller.
- 2) A new impedance algorithm was implemented to transfer stiffness from the human operator through by measuring user's force. This was then used to create the exoskeleton system's impedance model, which helps to compensate for human muscle force activities during rehabilitation tasks.
- 3) A new disturbance observer was developed, taking into consideration the absence of the accurate knowledge of exoskeleton's dynamics and the unknown saturation effects in robot's actuators.

The structure of this paper is organized as follows: The kinematics and dynamics model of the rehabilitation robot is given in section II. The approach design of the control is described in section III, which also involves many vital remarks. Section IV presents the illustrative experimental results confirming the proposed strategy. Finally, the conclusion as future work is given in section V.

II. SPECIFICATION OF EXOSKELETON ROBOT

A. ETS-MARSE Design

Rehabilitation robots have human-like anatomy to rehabilitate and ease human upper limb movement. The proposed ETS-MARSE (*École de Technologie Supérieure - Motion Assistive Robotic-exoskeleton for Superior Extremity*) robot can be worn by the human body and has synchronized movements with human motion. It is worth noting that the structural idea of the ETS-MARSE was inspired from the human arm anatomy and was designed to be in accordance with exoskeleton wearers undergoing physiotherapy.

Fig 1 shows the structure of the redundant ETS-MARSE with 7-DOFs. The scapulohumeral portion (shoulder portion) responsible for performing a variety of upper-limb movements is shown in Table I along with forearm movements. The vertical and horizontal extension/flexion movement of the scapulohumeral is ensured by the first two joints, while the third joint is designed to assist the internal and external rotation of the shoulder. The elbow portion is designed as a single joint used to complete the flexion/extension motion of the elbow. The wrist, last part of the upper limb, is composed of three joints: The first is dedicated to perform pronation and supination motion of the forearm, while the second and third joints are used to accomplish two movements respectively: ulnar/radial deviation and flexion/extension motion.

Compared to existing exoskeleton robots, ETS-MARSE has beneficial characteristics including excellent power/weight ratio, ease of usage, comparatively low weight, as well as being able to adequately compensate for gravity [33, 34].

TABLE I
WORKSPACE ETS-MARSE

Joints	Motion	Workspace
1	Shoulder joint horizontal flexion/extension	0°/140°
2	Shoulder joint vertical flexion/extension	140°/0°
3	Shoulder joint internal/external rotation	-85°/75°
4	Elbow joint flexion/extension	120°/0°
5	Forearm joint pronation/supination	-85°/85°
6	Wrist joint Ulnar/Radial deviation	-30°/20°
7	Wrist joint flexion/extension	-50°/60°

A high 6-axis force sensor (NANO17-R-1.8-M2-M1PCI, ATI industrial Automation) is selected to collect precise real-time force measurements. This sensor provides important feedback to reliably manage the exoskeleton robot in different modes of the rehabilitation protocol (passive, active and active-assisted). It is positioned on the tip of the exoskeleton robot. Table II presents the modified Denavit-Hartenberg (DH) parameters [35]. The reference frames for the settings are given in Fig. 1. Details of the physical parameters of ETS-MARSE can be found in the investigations done [9, 33].

TABLE II
MODIFIED DENAVIT-HARTENBERG PARAMETERS

<i>Joint (i)</i>	α_{i-1}	a_{i-1}	d_i	θ_i
1	0	0	d_s	θ_1
2	$-\pi/2$	0	0	θ_2
3	$\pi/2$	0	d_e	θ_3
4	$-\pi/2$	0	0	θ_4

5	$\pi/2$	0	d_w	θ_5
6	$-\pi/2$	0	0	$\theta_6 - \pi/2$
7	$-\pi/2$	0	0	θ_7

B. ETS-MARSE Dynamics Model

The dynamic of ETS-MARSE under saturation constraints is presented as follows:

$$M(\theta(t))\ddot{\theta}(t) + C(\theta(t), \dot{\theta}(t))\dot{\theta}(t) + G(\theta(t)) - f_{ex}(t) = \beta(\tau(t)) \quad (1)$$

where $\theta(t)$ denotes a 7-vector of generalized coordinates; $M(\theta(t)) \in R^{7 \times 7}$, $C(\theta(t), \dot{\theta}(t))\dot{\theta}(t) \in R^7$, and $G(\theta(t)) \in R^7$ are respectively inertia matrix, which is symmetric and bounded, Coriolis and centrifugal torques, and the gravitational torques. $\tau \in R^7$ is the torque input vector, $f_{ex}(t) = J^T f_h(t) \in R^7$ is the external force vector, with $f_h(t) \in R^6$ being the measured force and $J^T \in R^{6 \times 7}$ being the Jacobian matrix. The saturation restriction is expressed as follows:

$$\beta(\tau(t)) = \begin{cases} \beta_{max} \text{sign}(\tau), & |\tau| \geq \beta_{max} \\ \tau, & |\tau| < \beta_{max} \end{cases} \quad (2)$$

where β_{max} is the upper bound of torque for the control input $\tau \in R^7$, with $\beta(\tau) = [\beta(\tau_1) \cdots \beta(\tau_7)]^T$.

Without loss of generality, the human-robot interaction dynamics (1) can be rewritten as follows:

$$\begin{cases} M(\theta(t)) = M_0(\theta(t)) + \Delta M(\theta(t)) \\ C(\theta(t), \dot{\theta}(t)) = C_0(\theta(t), \dot{\theta}(t)) + \Delta C(\theta(t), \dot{\theta}(t)) \\ G(\theta(t)) = G_0(\theta(t)) + \Delta G(\theta(t)) \\ \beta(\tau(t)) = \tau(t) + \Delta \tau(t) \end{cases} \quad (3)$$

where $M_0(\theta(t))$, $C_0(\theta(t), \dot{\theta}(t))$, and $G_0(\theta(t))$ are the known parts of the inertia matrix, the Coriolis/centrifugal matrix, and the gravity vector respectively; while $\Delta M(\theta(t))$, $\Delta C(\theta(t), \dot{\theta}(t))$, and $\Delta G(\theta(t))$ are the uncertain parts. $\beta(\tau(t))$ is the nominal input, $\tau(t)$ is the torque input under saturation constraints, and $\Delta \tau(t)$ is the torque disturbance.

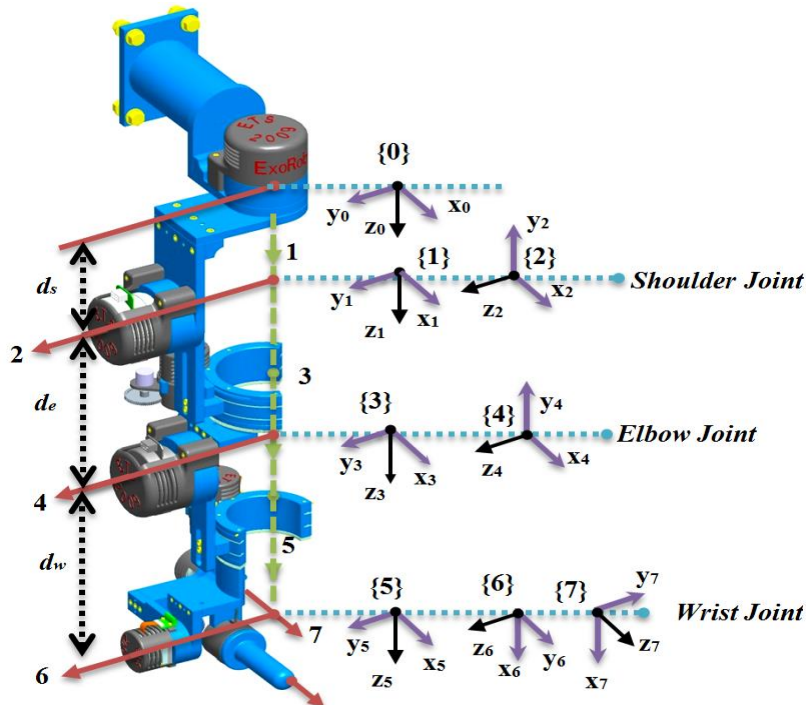


Fig. 1. ETS-MARSE exoskeleton robot.

By defining : $\eta_1 = \theta(t)$ and $\eta_2 = \dot{\theta}(t)$, the exoskeleton dynamic model represented by (1) can be rewritten such that::

$$\begin{cases} \dot{\eta}_1 = \eta_2 \\ \dot{\eta}_2 = U(t) + f(t) + H(t) + D(t) + f_{ex}(t) \end{cases} \quad (4)$$

where, $U(t) = M_0^{-1}(\theta)\tau(t)$

- $H(t) = M_0^{-1}(\theta)(-\Delta M(\theta)\ddot{\theta} - \Delta C(\theta, \dot{\theta})\dot{\theta} - \Delta G(\theta))$, and
- $f(t) = M_0^{-1}(\theta)(-C_0(\theta, \dot{\theta})\dot{\theta} - G_0(\theta))$
- $D(t) = M_0^{-1}(\theta)(\Delta\tau) + f_{ex}(t)$

C. Dynamics Model of the Human Upper Limb

This section is dedicated to designing an impedance control able to match the dynamic behavior of the user and the exoskeleton robot. The dynamic model of the human upper-limb is firstly defined as a second-order system (a desired mass-damper-spring system) as follows [36]:

$$M_h \ddot{\eta}_2 + C_h \dot{\eta}_2 + G_h \eta_1 = J^T f_h \quad (5)$$

where M_h, C_h and $G_h \in R^{7 \times 7}$ are the inertia, damping and spring matrices of the human end-effector, respectively. In such a case, the dynamics (5) are considered as an impedance model.

Remark 1: The position, velocity, and acceleration feedbacks of the human upper-limb are not available. It is acceptable to use the exoskeleton feedback since it can be worn by the human upper-limb and has synchronized movements with human motion.

By defining the error tracking of the position as $e = \eta_1 - \eta^d$ with $\eta^d \in R^7$ being the desired trajectory, the reference model (5) can be rewritten as follows:

$$M_h \ddot{e} + C_h \dot{e} + G_h e = -\zeta \quad (6)$$

with $\zeta = (M_h \ddot{\eta}^d + C_h \dot{\eta}^d + G_h \eta^d - J^T f_h)$. The goal here is to design a suitable control input torque τ where the exoskeleton dynamics can overlap with the reference impedance model given by Eq. 5. Taking into consideration the deviation between the exoskeleton dynamics and the reference impedance model, the matching error can be introduced such that:

$$\phi(t) = M_h \ddot{e} + C_h \dot{e} + G_h e + \zeta \quad (7)$$

So, when $\lim_{t \rightarrow \infty} \phi(t) = 0$, the exoskeleton dynamic model (4) will able to perfectly match the reference impedance model (5)". To facilitate the presented analysis, the augmented matching error (7) can be defined as:

$$\bar{\phi}(t) = K_\zeta \phi(t) = \ddot{e} + K_d \dot{e} + K_p e + K_\zeta \zeta \quad (8)$$

where $K_\zeta = M_h^{-1}$, $K_d = M_h^{-1}C_h$ and $K_p = M_h^{-1}G_h$. Choosing two positive definite matrices $\Lambda(e)$ and Π fulfilling $(\Lambda(e) + \Pi) = K_d$ and $(\Lambda(e) \Pi + \dot{\Lambda}(e)) = K_p$, the augmented matching error (8) can be rewritten as follows:

$$\bar{\phi}(t) = \ddot{e} + (\Lambda(e) + \Pi)\dot{e} + (\Lambda(e) \Pi + \dot{\Lambda}(e))e + \dot{\xi}_i + \Pi \zeta_i \quad (9)$$

where ζ_i satisfies $K_\zeta \zeta = \dot{\xi}_i + \Pi \zeta_i$; and $\Lambda(e) = \text{diag} \left[K_{ii} \left(1 - e^{-\frac{|e_i|}{\epsilon_i}} \right) \right]$, with $i = 1, \dots, 7$; where $K_{ii} > 0$ and $\epsilon_i > 0$. The variation of $\Lambda(e)$ is based on the variation of the error (e) for which $\Lambda(e)$ should always be strictly positive. If the error (e) increases, $\Lambda(e)$ will also increase, forcing the error (e) to converge to zero. Consequently, as (e) decreases, $\Lambda(e)$ will converge to zero. Introducing a new variable s as filtered matching error:

$$s = \dot{e} + \Lambda(e)e + \zeta_i \quad (10)$$

Then the augmented error Eq. 9 can be reformulated as follows using Eq.10:

$$\bar{\phi}(t) = \dot{s} + \Pi s \quad (11)$$

So, $\lim_{t \rightarrow \infty} s(t) = 0$ drives $\lim_{t \rightarrow \infty} \dot{s}(t) = 0$; supposing that $\lim_{t \rightarrow \infty} \dot{s}(t) = 0$ exists. Taking into consideration Eq. 8 and Eq. 9, $\lim_{t \rightarrow \infty} \phi(t) = 0$ if $\lim_{t \rightarrow \infty} s(t) = 0$. In this case, the goal of the control will be reached by achieving:

$$\lim_{t \rightarrow \infty} s(t) = 0 \quad (12)$$

which means that objective (7) can be reduced to zero. The properties and assumptions employed in this research are described such that:

Property 1: The known inertia matrix part $M_0(\theta)$ is symmetric, positive definite, and bounded for all $\theta \in R^7$.

Assumption 1: The function $H(t)$ is locally Lipschitz function.

Assumption 2: The reference trajectory is bounded.

Assumption 3: The disturbance f_{ex} is assumed to be continuous, bounded, and fulfils $\|f_{ex}\| \leq \varepsilon$, with ε being an unknown positive boundary.

Lemma 1: [37] Let Lyapunov function $V(y)$ be continuous and positive definite, realizing $\lambda_1(\|y\|) \leq V(y) \leq \lambda_2(\|y\|)$ and its derivative $\dot{V}(y) = dV(y)/dt$ and satisfying $\dot{V}(y) \leq -\alpha_1 V(y) + \alpha_2$, where α_1 and α_2 are positive constants. Therefore the solution $y(t)$ is bounded.

Lemma 2: A function $\omega(t)$ is continuous and differentiable bounded, $\forall t \in [t_0, t_1]$, if $\omega(t)$ fulfills $|\omega(t)| \leq \delta$, where δ is a positive constant, therefore $\dot{\omega}(t)$ is bounded. See proof in Appendix-A

Remark 2: The $\omega(t)$ in Lemma 2 is not a piecewise function. On the contrary, remarks 3 and 4 will give more clarification about the piecewise function that was given in Eq. 2.

III. CONTROL DESIGN

In this section, a control strategy capable of completing the passive rehabilitation movement is developed. In such a case, the exoskeleton carries the upper arm of the subject to perform the physical therapy task. This section will be divided into two subsections.

A. Model-Based Control of the exoskeleton robot

The goal of this subsection is to establish a tracking control that can reduce unexpected disturbances saturation effects, with the goal of achieving the desired performance. In this section $H(t)$ is assumed to be known while D is unknown. The required velocity and acceleration are defined as follows:

$$\begin{cases} \dot{\eta}_r = \dot{\eta}^d - \Lambda(e)e - \zeta_i \\ \ddot{\eta}_r = \ddot{\eta}^d - \dot{\Lambda}(e)e - \Lambda(e)\dot{e} - \dot{\zeta}_i \end{cases} \quad (13)$$

Based on Eq. 10, the following can be obtained:

$$\begin{cases} \dot{\eta}_1 = \dot{\eta}_r + s \\ \dot{\eta}_2 = \dot{\eta}_r + \dot{s} \end{cases} \quad (14)$$

Next, the regulated errors variables are chosen as follows:

$$e_1 = e = \eta_1 - \eta^d \quad (15)$$

$$e_2 = \eta_2 - \dot{\eta}_r \quad (16)$$

Step 1: Differentiating Eq.15 results with:

$$\dot{e}_1 = \dot{\eta}_1 - \dot{\eta}^d = e_2 + \dot{\eta}_r - \dot{\eta}^d = e_2 - \Lambda(e)e_1 - \zeta_i \quad (17)$$

From the Eq. 16, the following can be found:

$$e_2 = s + \dot{\eta}_r - \dot{\eta}_r = s \quad (18)$$

Consider the first Lyapunov function candidate as follows:

$$V_1 = \frac{1}{2} e_1^T e_1 \quad (19)$$

Differentiating V_1 results with:

$$\dot{V}_1 = e_1^T \dot{e}_1 = e_1^T (e_2 - \Lambda(e) e_1 - \zeta_l) \quad (20)$$

Step 2: Differentiating Eq. 18, results with:

$$\dot{e}_2 = \dot{s} = U(t) + f(t) + H(t) + D + f_{ex}(t) - \ddot{\eta}_r \quad (21)$$

Due to the known terms $\Delta\tau$, the disturbance D is unknown term. Considering Lemma 2, Eq. 2, and property 1, the following inequality becomes true:

$$\|\dot{D}\| \leq \sigma \quad (22)$$

where σ is an unknown positive constant.

Remark 3: Using Lemma 2, the functions $\beta_{max} \text{sign}(\tau)$ and τ of saturation restrictions determined in Eq. 2 are piecewise functions. Two cases can be obtained: The first is that the control input τ reaches its bound β_{max} based on the expressions of saturation restrictions (Eq. 2), and $\beta(\tau)$ remains bounded and constant; then, $\Delta\tau = \beta(\tau) - \tau$ with the desired continuous control input τ is fulfilling the condition of **Lemma 2**. The second is that if the motor does not reach the saturation limit, its outputs are continuous and smooth with $\Delta\tau = 0$. So, the term D is used to estimate the disturbances in this case. Incorporating both instances, the term $\Delta\tau$ can be obtained, which would always fulfill **Lemma 2**.

Next, the disturbances' nonlinear observer can be established to approximate the term D . Firstly, the auxiliary error is defined such that:

$$e_3 = D - k_3 e_2 \quad (23)$$

where $k_3 = \text{diag}(k_{31} \dots k_{37}) > 0$ and $i = 1, \dots, 7$. The derivative of e_3 from Eqs. 22 and 23 is:

$$\begin{aligned} \dot{e}_3 &= \dot{D} - k_3 \dot{e}_2 \\ &= \dot{D} - k_3 [U(t) + f(t) + H(t) + f_{ex}(t) + D] + k_3 \ddot{\eta}_r \end{aligned} \quad (24)$$

Due to the unavailability of the term D , the variable e_3 also vanishes. To estimate e_3 , a dynamical system of an estimator is proposed such:

$$\dot{\hat{e}}_3 = -k_3 [U(t) + f(t) + H(t) + f_{ex}(t) + \hat{D}] + k_3 \ddot{\eta}_r \quad (25)$$

where \hat{e}_3 is the estimated value of e_3 . From Eq. 23, the value of the disturbance D can be obtained such that:

$$\hat{D} = \hat{e}_3 + k_3 e_2 \quad (26)$$

The following can then be obtained:

$$\tilde{e}_3 = e_3 - \hat{e}_3 = D - \hat{D} = \tilde{D} \quad (27)$$

The time derivative of Eq. 27, taken into consideration Eqs. 24 and 25, gives:

$$\dot{\tilde{D}} = \dot{\tilde{e}}_3 = \dot{e}_3 - \dot{\hat{e}}_3 = \dot{D} - k_3 \tilde{D} \quad (28)$$

The proposed model-based control input that stabilizes the system is given by:

$$U(t) = -k_2 e_2 - e_1 - f(t) - H(t) - f_{ex}(t) - \hat{D} + \ddot{\eta}_r \quad (29)$$

with, $\tau = M_0(\theta)U(t)$; and $k_2 \in R^{7 \times 7}$ is a diagonal positive-definite matrix. If the following conditions are satisfied:

$$\begin{cases} k_2 - \frac{1}{2} I_{7 \times 7} > 0 \\ k_3 - I_{7 \times 7} > 0 \end{cases} \quad (30)$$

Theorem 1: The designed model-based control (29) for the human-robot interaction dynamics (1), which satisfies Assumptions (3-4) and Lemmas (1-2), using the impedance model (6), renders the whole system including its bounded error signals e_1 , e_2 and \tilde{e}_3 as asymptotically stable according to Lemma 1.

Proof: The detailed proof of Theorem 1 is presented in Appendix B.

B. Adaptive Time Delay Controller

Evidently, it is challenging to obtain exoskeleton dynamic models due to the aforementioned uncertainties and disturbances, particularly, during exoskeleton motion. Since $H(t)$ is uncertain, it may affect the control scheme, in which the control input (29) is infeasible. To surmount this, the TDE approach [24] is used to estimate the uncertainties of the nonlinear robot dynamics. As such, if Assumption 1 holds, the term $H(t)$ can be estimated from Eq. 4 such that:

$$\hat{H}(t) \approx H(t - t_d) = \dot{\eta}_2(t - t_d) - f(t - t_d) - f_{ex}(t - t_d) - U(t - t_d) - \hat{D}(t - t_d) \quad (31)$$

where t_d is a very short time delay constant. In real time, the sampling time is the smallest constant that can be realized. Nevertheless, because of the complex nonlinearity of the human-robot interaction dynamics during delay constant, a TDR (ε) exists. Based on Lipschitz condition (Assumption 1), it can be defined as follows:

$$\begin{aligned} \tilde{H}_i(t) &= \varepsilon_i = H_i(t) - \hat{H}_i(t) \\ &= H_i(t) - H_i(t - t_d) \leq \varrho_i t_d \end{aligned} \quad (32)$$

where $\varrho_i > 0$ is a Lipschitz constant with $i = 1 \dots 7$. This TDR would degrade the approximation performance. Regrettably, the TDR is not obtainable. In this case, the TDR can be combined with the disturbances, which are both then used by the nonlinear observer to reduce such effects. As such, the new combined disturbance D can be formulated as:

$$D = M_0^{-1}(\theta)(\Delta\tau - \varepsilon) \quad (33)$$

According to the equation (32), the TDR ε is bounded and satisfies Lemma 2, which implies Eq. 22 ($\|\dot{D}\| \leq \sigma$).

Remark 4: In addition to both cases of Remark 3, it is essential to know that the Time Delay Error ε is always bounded. According to Lemma 2, $\|\varepsilon\|$ is also bounded.

Again, a nonlinear observer of the combined disturbances D can be designed with the objective to estimate such disturbances; defining again the auxiliary error such that:

$$e_3 = D - k_3 e_2 \quad (34)$$

where $k_3 = \text{diag}(k_{31} \dots k_{37}) > 0$ and $i = 1, \dots, 7$. The time derivative of e_3 from Eqs. 21 and 34 becomes:

$$\begin{aligned} \dot{e}_3 &= \dot{D} - k_3 \dot{e}_2 \\ &= \dot{D} - k_3[U(t) + f(t) + H(t) + f_{ex}(t) + D] + k_3 \ddot{\eta}_r \end{aligned} \quad (35)$$

As in the previous subsection, e_3 is unavailable because of the unknown variables $H(t)$ and D . The estimated value of e_3 is given as follows:

$$\hat{\dot{e}}_3 = -k_3[U(t) + f(t) + \hat{H}(t) + \hat{D}] + k_3 \ddot{\eta}_r \quad (36)$$

where \hat{e}_3 is the estimated value of e_3 . From Eq. 34, the value of the disturbances D can be obtained as:

$$\hat{D} = \hat{e}_3 + k_3 e_2 \quad (37)$$

From which, it clearly then follows that:

$$\tilde{e}_3 = e_3 - \hat{e}_3 = D - \hat{D} = \tilde{D} \quad (38)$$

The time derivative of Eq. 38, from Eqs. 35-36 gives:

$$\dot{\tilde{D}} = \dot{\tilde{e}}_3 = \dot{e}_3 - \dot{\hat{e}}_3 = \dot{D} - k_3(\tilde{D} + \tilde{H}) \quad (39)$$

The proposed adaptive time delay controller that can ensure the stability of the system becomes :

$$U(t) = -k_2 e_2 - e_1 - f(t) - f_{ex}(t) - \tilde{H}(t) - \tilde{D} + \ddot{\eta}_r \quad (40)$$

with, $\tau = M_0(\theta)U(t)$. If the following conditions are satisfied:

$$\begin{cases} k_2 - I_{7 \times 7} > 0 \\ k_3 - \frac{3}{2} I_{7 \times 7} > 0 \end{cases} \quad (41)$$

Theorem 2: For human-robot interaction dynamics (1) characterized by impedance model (6), and satisfies Assumptions (3-4) and Lemmas (1-2), the implementation of a designed adaptive control scheme (40) that is based on TDE and (31) augmented with the rejection observer of disturbances (37) ensures the stability of the system whereby all its error signals e_1, e_2, \tilde{H} and \tilde{e}_3 are bounded according to Lemma 1.

Proof: The detailed proof of Theorem 1 is presented in Appendix C.

The diagram of the designed control scheme is presented in Fig. 2.

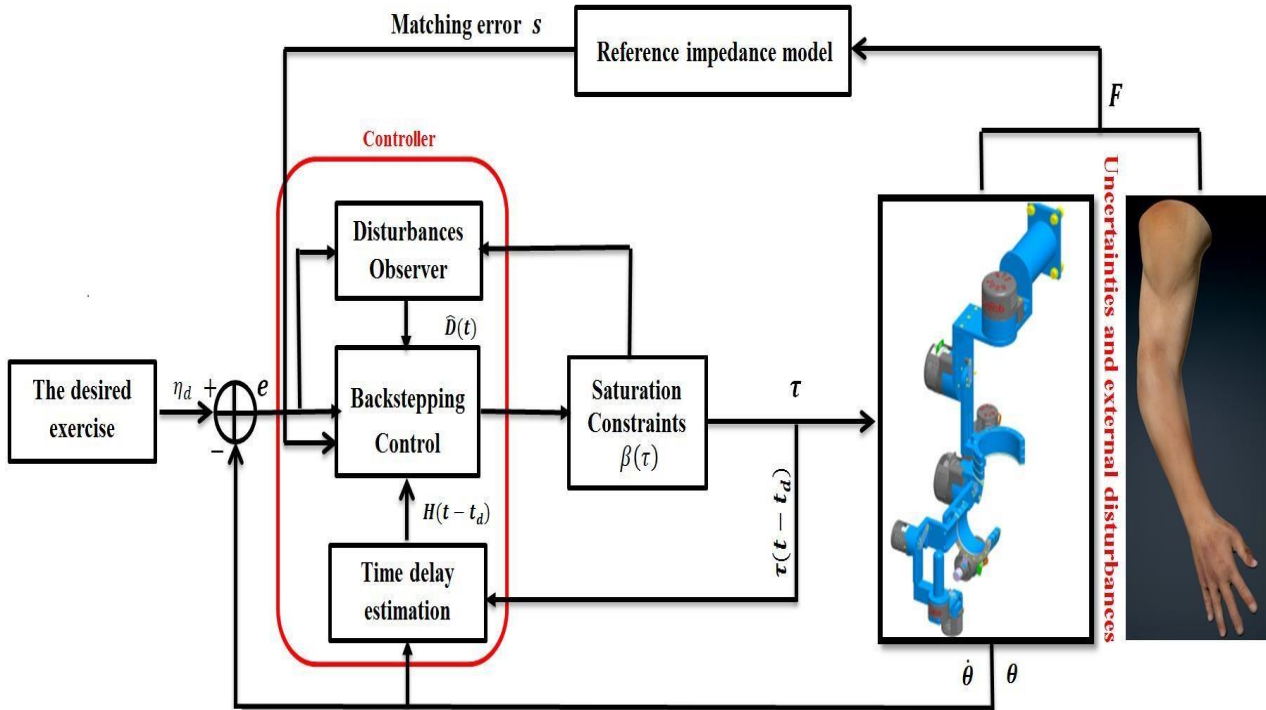


Fig. 2. The diagram of the proposed controller.

IV. EXPERIMENT AND COMPARATIVE STUDY

A. Experiment Description

ETS-MARSE real-time system is composed of three processing units: The first is the computer (PC) where the top-level control is sent to the robot using a human-machine interface through LabVIEW 2017. The other two processing units are parts of a National Instruments PXI unit: The second unit is NI-PXI 8081 controller board, where the top-level control is executed at a sampling time of $500 \mu\text{s}$. The last one is NI PXI-7813R remote input/output board with a Field Programmable Gate Array (FPGA) that executes the low-level control (PI) current control loop (sampling time of $50 \mu\text{s}$) to ensure that the necessary current, required by the top level controller, is fed to the motors. The joints of the robot are powered by Brushless DC motors (Maxon EC-45 and Maxon EC-90) combined with harmonic drives (a gear ratio of 120:1 for motors 1 and 2; and a gear ratio of 100:1 for motors 3-7) [34, 38]. The components of the experiment platform are shown in Fig. 3.

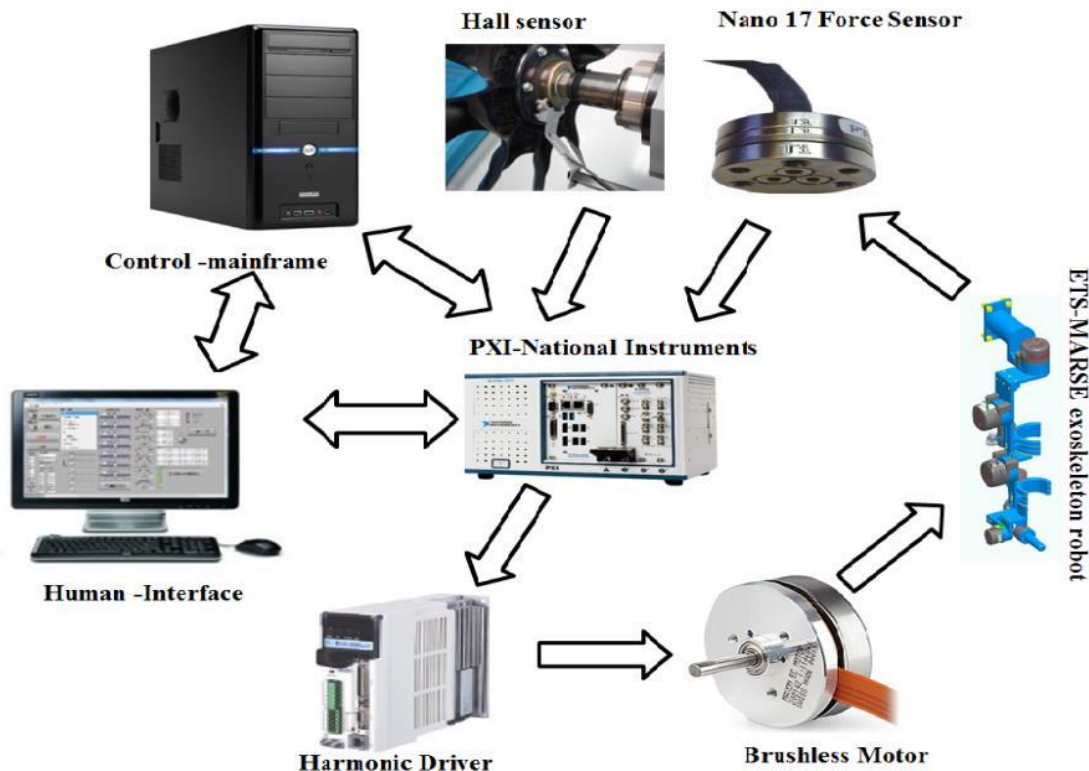


Fig. 3. Experimental platform.

A passive rehabilitation therapy analysis, composed of four different scenarios, has been conducted by two healthy subjects to show the efficiency of the proposed controller. The first scenario, elbow joint flexion/extension and forearm pronation/supination, was executed by the exoskeleton by subject-1 (age: 27 years; height: 170 cm; weight: 75 kg), using backstepping controller based on TDE [32]. In the second scenario, subject-1 repeated the same exercise using the designed controller (40). The third was dedicated to investigating the effect of a conventional PID controller, which does not require the dynamic mode of the exoskeleton robot. This was achieved by subject-1 repeating the same movement of the previous exercise. Lastly, the proposed approach in Cartesian space, performed by healthy subject-2 (age: 31 years; height: 178 cm; weight: 80 kg) was investigated. This was done to show how does the proposed controller reacts to different variabilities, such as other physiological situations of the exoskeleton's wearers and changing upper-limbs mass. A 90 degrees elbow joint position was assumed as an initial position of the exoskeleton robot.

B. Experiment Results

Scenario 1: The backstepping tracking control was implemented with Time Delay Estimation [32], where the dynamic model of the exoskeleton is not entirely known. Subject-1 (age: 27 years; height: 170 cm; weight: 75 kg) performed basic elbow joint flexion/extension and forearm pronation/supination using ETS-MARSE robot. The control parameters were chosen manually, based on trial and error, such that: $K_{ii} = 15$, $\epsilon_i = 3$ and $k_2 = 34.8I_{7 \times 7}$. Saturation boundaries were selected for the two motors as follows: $\beta_{1\max} = 4.15 \text{ Nm}$, $\beta_{2\max} = 4.15 \text{ Nm}$.

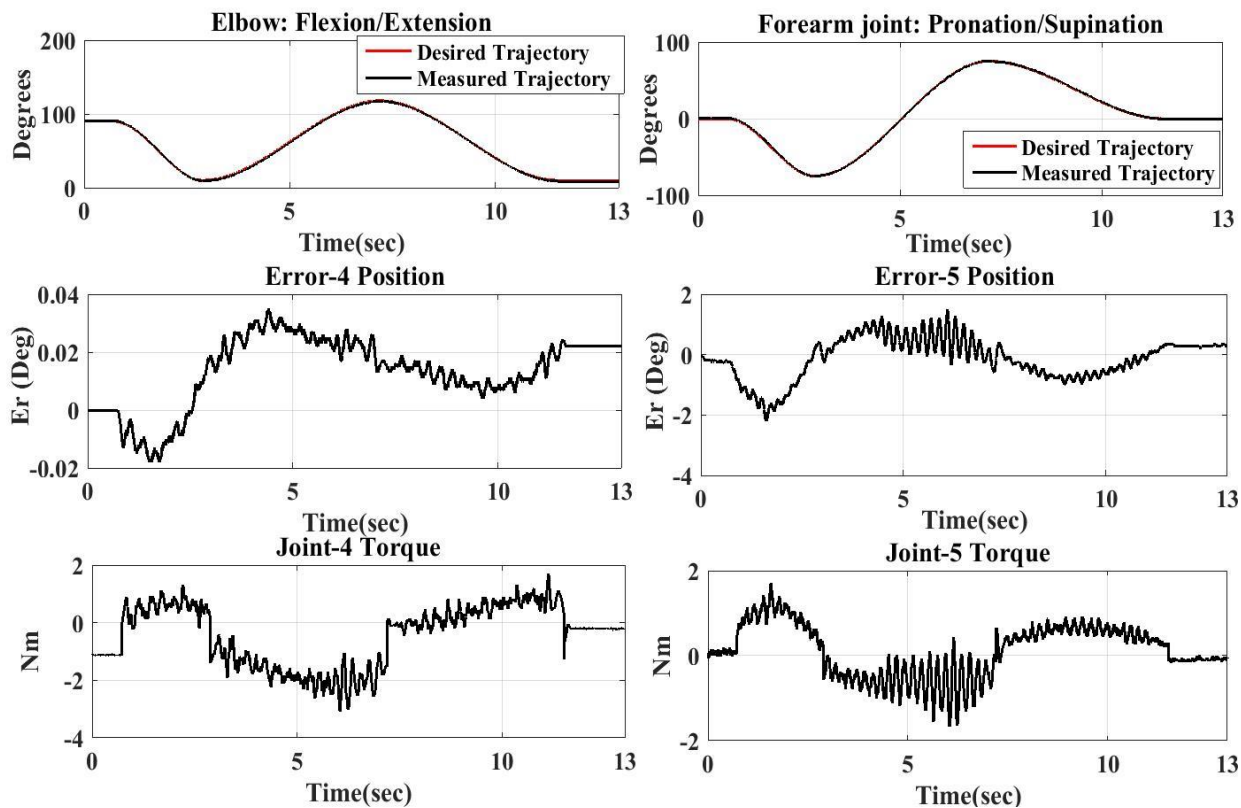


Fig. 4. Tracking of elbow joint position. (First column), Tracking of forearm joint position (Second column) (The red line is the desired trajectory and the black line is the measured trajectory) performed by subject-1 (Age: 27 years; height: 170 cm; weight: 75 kg).

Discussion 1: The experimental results of the exoskeleton robot, performed by subject-1 (Age: 27 years; height: 170 cm; weight: 75 kg), are presented in Fig. 4 using backstepping controller based on TDE. Fig. 4 shows that the reference trajectory (Red line) overlapped with the measured position (Black line). The last two sets of data (Fig. 4) present the tracking errors and the control input, respectively. In this test, the proposed controller provided the desired physical therapy even though the dynamical model of the robot was unknown. However, undesirable chattering, caused by uncertainties and subject behavior (Saturation, payload, and human muscle conditions), still appeared.

Scenario 2: The designed backstepping control (40), augmented with human impedance model, and incorporating the designed disturbance observer was implemented. In this test, the same control parameters of the previous scenario were adopted. On the other hand, the designed observer control parameters have been tuned, based on trial and error, such that: $k_3 = 0.08I_{7 \times 7}$. Saturation boundaries were selected for the two actuators as follows: $\beta_{1\max} = 4.15 \text{ Nm}$, $\beta_{2\max} = 4.15 \text{ Nm}$.

Discussion 2: The experimental results of the exoskeleton robot conducted by the same subject are shown in Fig. 5 using the proposed control strategy. It is obvious from Fig. 5 that the measured position (Black line) is also identical to the reference trajectory (Red line). Tracking errors and control inputs are shown respectively by the last two sets of data (Fig. 5). The evolution of the disturbance observer output is presented in Fig. 6. Two key observations can be made: Firstly, the control inputs (third set of data of Fig. 5) are relatively smaller and smoother (without chattering) than the control inputs of the first scenario (third set of data of Fig. 4). Furthermore, it is evident that the high frequency of the control inputs has been actively reduced, with an improvement in the tracking trajectory caused by the integration of the proposed disturbance observer output. These remarks prove the feasibility of the proposed control and the efficiency behind combining the time delay estimation with the disturbance observer.

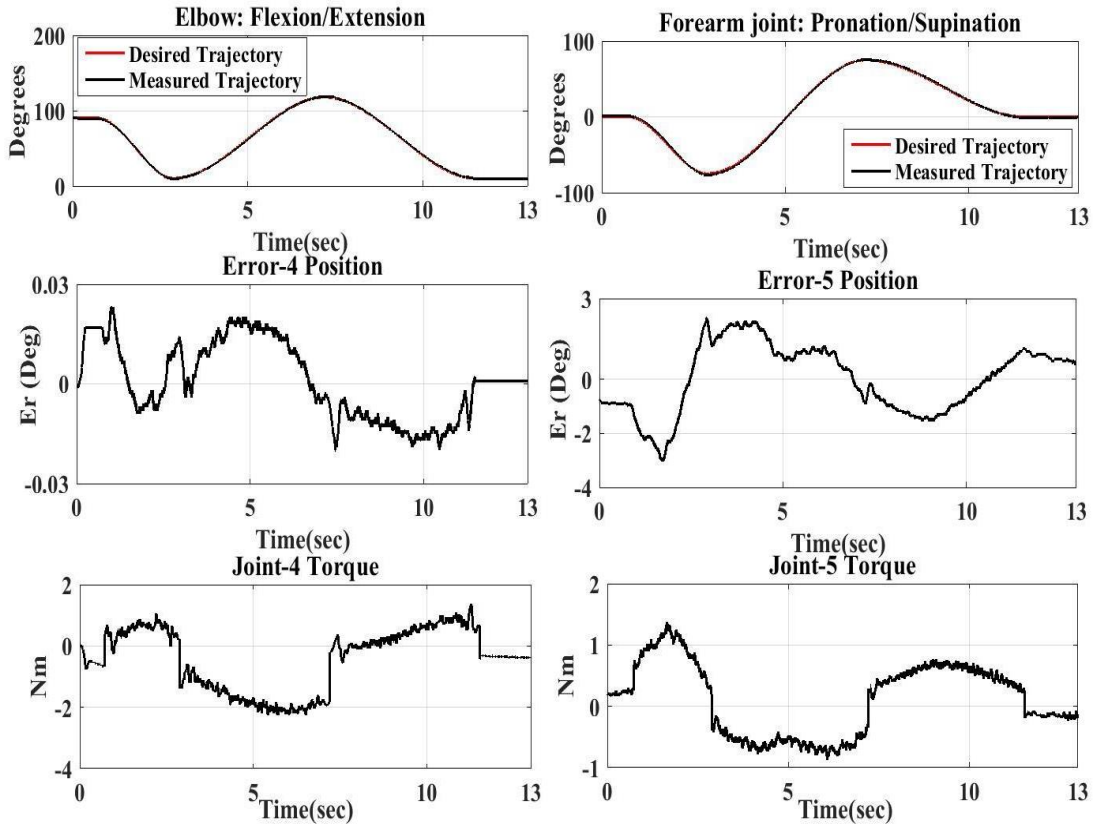


Fig. 5. Tracking of elbow joint position (First column). Tracking of forearm joint position (second column). The red line represents the desired trajectory while the black one represents the measured trajectory.

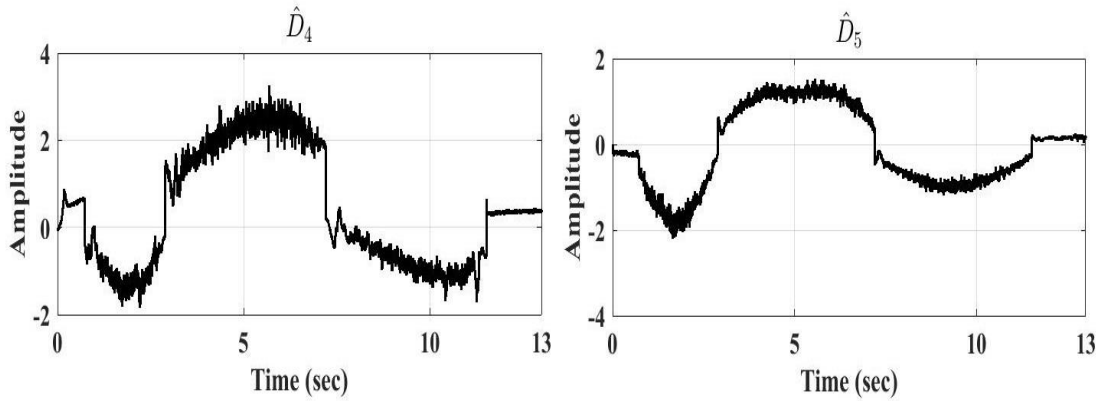


Fig. 6. The outputs of the disturbance observer.

Scenario 3: A comparison with PID control strategy was made to further prove the feasibility of the proposed approach. The adopted PID control is given by $\tau = \ddot{\eta}_d - K_p e - K_i \int e - K_d \dot{e}$. The associated gains were manually chosen, based on trial and error, such that: $K_p = 150I_{7 \times 7}$, $K_i = 100I_{7 \times 7}$ and $K_d = 80I_{7 \times 7}$. Saturation limits for the two motors are given as follows: $\beta_{1\max} = 4.15 \text{ Nm}$, $\beta_{2\max} = 4.15 \text{ Nm}$. The experimental results are presented in Fig. 6.

Discussion 3: Fig. 7 represents the performance of the exoskeleton robot, as performed by subject-1, using the PID controller. As depicted in the figure, in terms of error tracking for joint 5, the PID controller seemed to perform better than the proposed one. On the contrary, it is evident that the proposed approach was better and smoother than the PID in the case of controlling joint 5 input (torque input). Based on the gains value of the PID and proposed control methods, it can be concluded that the proposed controller was able to achieve a higher performance, with smaller gains, compared to PID. Furthermore, the control input of the proposed strategy is relatively smoother than the results presented by the PID controller. Thus, the designed controller is highly efficient when considering the unknown dynamics, time delay error, and saturation point constraint.

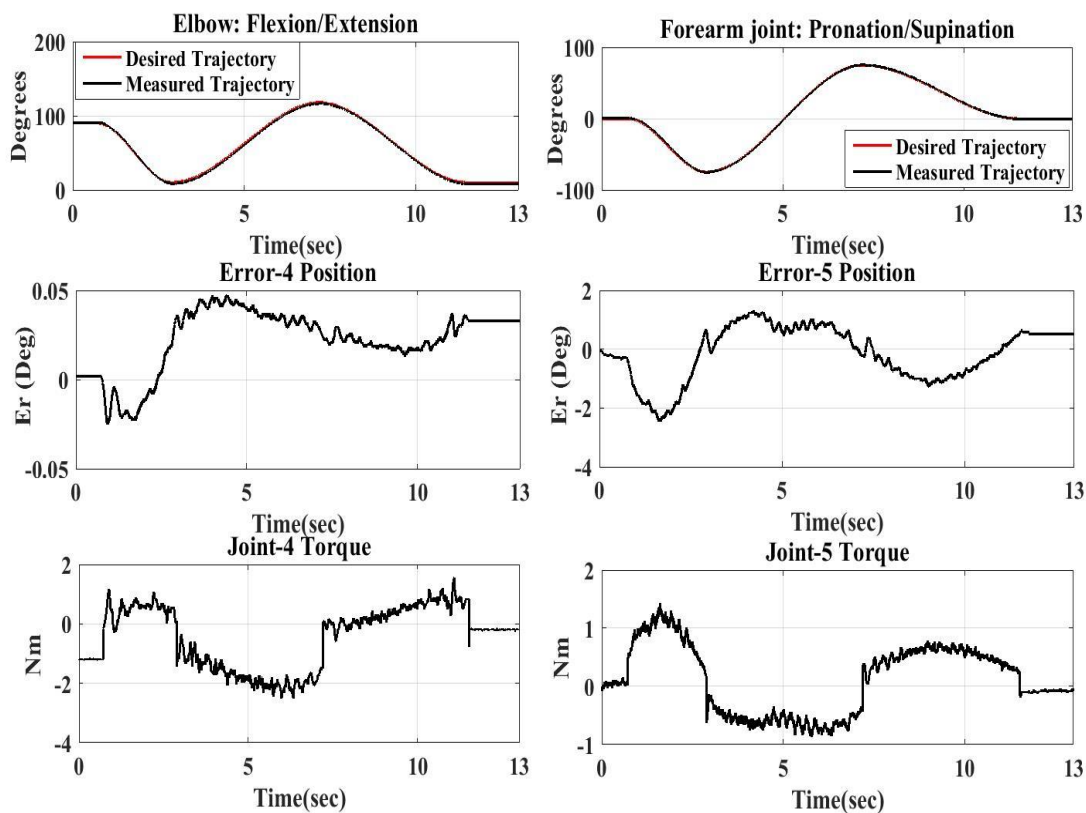


Fig. 7. PID controller results: Tracking of elbow joint position(First column). Tracking of shoulder joint position (second column). The red line represents the desired trajectory while the black one represents the measured trajectory. .

Scenario 4: The robot, as controlled by the proposed method, was tested by the second healthy subject-2 (age: 31 years; height: 178 cm; weight: 80 kg). This was primarily done to show how does the proposed controller reacts to different variabilities, such as other physiological situations of the exoskeleton's wearers and changing upper-limbs mass . The task starts at the initial position mentioned earlier (90 degrees of elbow angle). Then, the end-effector follows a path until it reaches target 'A', another path from 'A' to 'B', followed by the path from target 'B' to target 'C', until if finally returns to the initial position (Fig. 8). The same control parameters used in this scenario are the ones adopted in the second one.

Discussion 4: The results of the task conducted by subject-2 (age: 31 years; height: 178 cm; weight: 80 kg) are illustrated in Figs. 8-10. The desired rotation of the end-effector is considered zero. As depicted by Fig. 8, the path subject-2 followed, the achieved cartesian movement, denoted by the desired trajectory and represented by the red line, realistically overlaps with the measured trajectory, given by the black line. The excellent performance of the designed controller is highly noticeable for which it has kept stability along the whole duration of the desired trajectory with a very small margin of error(Fig. 9). Furthermore, the control inputs are acceptable as shown in Fig. 10.

Robot End Effector Desired and Measured Trajectory

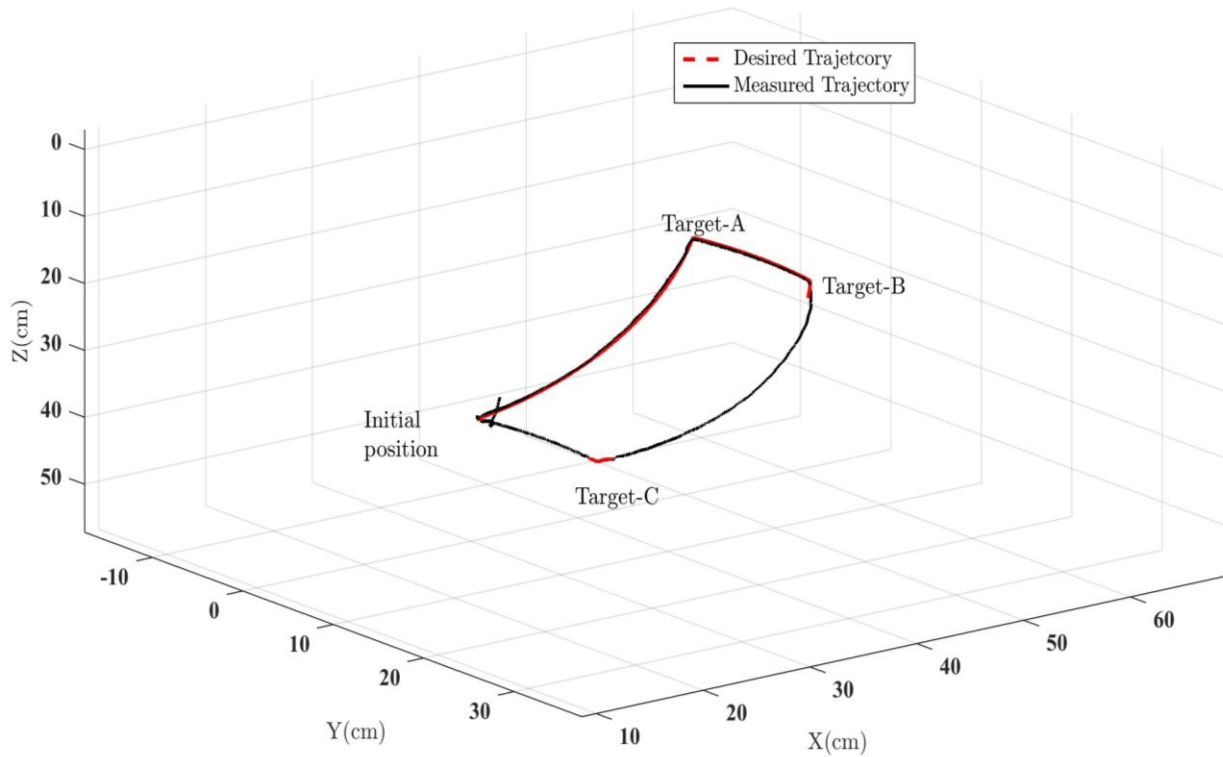


Fig. 8. Tracking of the exoskeleton, with the task performed by subject-2, in cartesian space (red line represents the desired trajectory while the black one represents the measured trajectory) using the proposed approach.

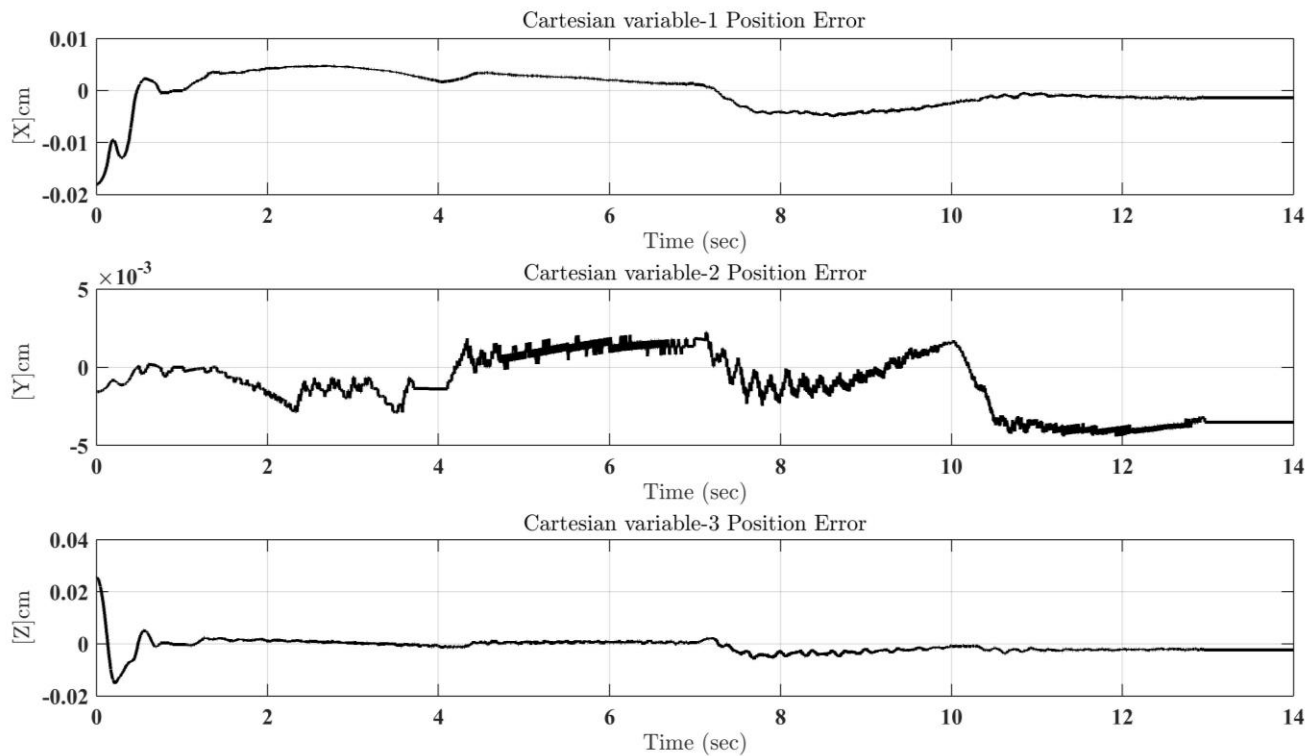


Fig. 9. Evolution of the cartesian errors.

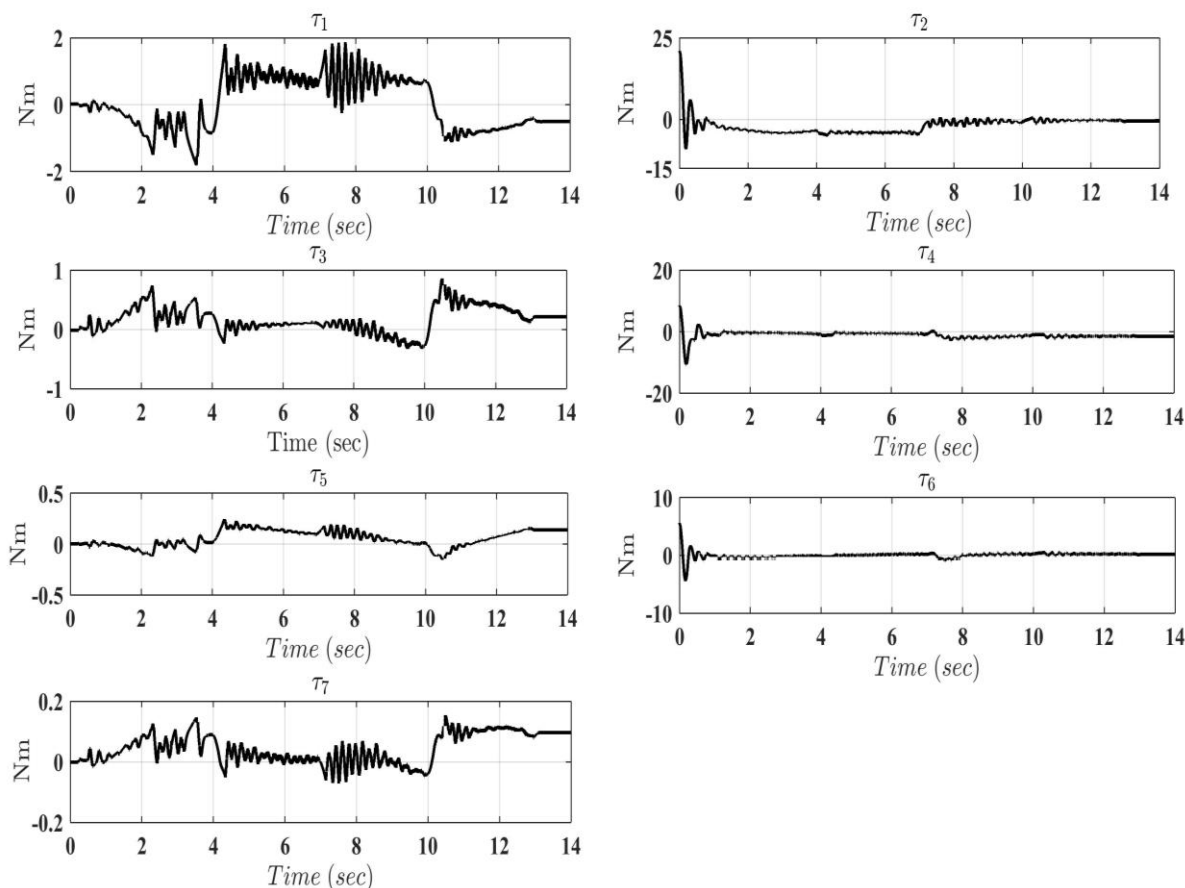


Fig. 10. Evolution of the control input.

C. Comparison study

In order to evaluate the reliability of the proposed control scheme, the performance of the proposed controller was evaluated for different subjects (different arm weights, different physiological conditions, and altered states of mind). The sensitivity of the approach when removing the disturbance observer was also assessed by calculating the root mean square (RMS) of each error and the total energy consumed in joint space.

Table. III Controller sensitivity parameters

Subjects	root mean square (RMS) of errors			
	proposed Controller with the observer		proposed Controller without the observer	
	$\ e\ _{RMS\ error}$	$\ \tau\ _{RMS\ Torque}$	$\ e\ _{RMS\ error}$	$\ \tau\ _{RMS\ Torque}$
Subject-1	0.0018	1.3792	0.0395	2.2147
Subject-2	0.0032	1.9756	0.0352	2.3827

Clearly, from Table III, the proposed control scheme provides consistent performance with respect to different subjects. This was obvious as the RMS error and general torque input slightly changed when compared to the controller without the observer. Furthermore, in efforts of further validation, when comparing the results to similar literature investigations [34, 38], the proposed controller showed identical performance as the Virtual Decomposition Control [38], and a potentially better performance than the PID and Computed Torque Control [38]. These results are highly desirable since they are suitable to be used in the next phase of our project: Testing with stroke patients who could benefit from such assistive active and passive arm guidance rehabilitation. These results demonstrate the efficiency and suitability of the proposed controller scheme.

V. CONCLUSION

In closing, a new adaptive impedance control approach augmented with backstepping control was implemented on ETS-MARSE, a rehabilitative exoskeleton robot, and has shown to perform accurately for passive rehabilitation motion applications. The proposed control scheme used an impedance algorithm to transfer the stiffness of the human upper limb to the designed impedance model via measured user force from the exoskeleton system. As for the unknown dynamic parameters of the robot and unexpected disturbances, such as constraints of input saturation of the manipulator's motors, the notion of combining time delay estimation and a disturbance observer has been introduced in order to approximate and reject such disturbances. The disturbance observer output was directly connected to the adaptive Time Delay control using a feedforward loop, which permits the system to actively and quickly diminish these disturbances. Using this approach, the control input neither needs any precise knowledge of the exoskeleton dynamic model anymore, nor any necessary knowledge of built-in torque sensing units to achieve the desired performance. Experimental tests and results obtained using the ETS-MARSE and two healthy subjects demonstrated the advantages and benefits of the designed strategy of the present work. In future work, the authors are looking forward to 1) integrating an optimization approach to optimally select the control parameters of the proposed control; 2) incorporating other sensors of forces feedback such that Electromyography signals (EMGs) to detect the human muscles activities; and finally, 3) applying the proposed control to achieve different rehabilitation protocols such as active and active-assisted rehabilitation protocols.

ETHICS STATEMENT

In this research, ethics approval was not required as per École de Technologie Supérieure, Montreal, Canada and national regulations since the Subjects are healthy (not real neurological patients) and no subjects were recruited other than the researchers working on this project. Also, written and informed consent was obtained from the research participants.

APPENDIX

A. Proof of Lemma2

Based on the mean value theorem, for any $[a, b] \in [t_0, t_1]$, we have $\omega(b) - \omega(a) = \dot{\omega}(\varphi)(b - a)$ given any $\varphi \in [a, b]$. Since $|\dot{\omega}(\varphi)| \leq \delta$, $-\delta \leq \omega(b) - \omega(a) \leq \delta$, it is straightforward to find that the derivative $\dot{\omega}(\varphi)$ is bounded. While $[a, b]$ can be selected as any small interval on $[t_0, t_1]$, it can be found that $\dot{\omega}(t)$ is bounded $\forall t \in [t_0, t_1]$.

B. Proof of Theorem 1

Consider the second Lyapunov function candidate as:

$$V_2 = V_1 + \frac{1}{2}e_2^T e_2 + \frac{1}{2}\tilde{e}_3^T \tilde{e}_3 \quad (42)$$

where $\tilde{e}_3 = \tilde{D}$. Differentiating V_2 , the following can be obtained:

$$\begin{aligned} \dot{V}_2 &= e_1^T (e_2 - \Lambda(e)e_1 - \zeta_l) + e_2^T \dot{e}_2 + \tilde{D}^T \dot{\tilde{D}} \\ &= e_1^T (e_2 - \Lambda(e)e_1 - \zeta_l) + e_2^T (U(t) + f(t) + H(t) + f_{ex}(t) + D - \dot{\eta}_r) + \tilde{D}^T \dot{D} - \tilde{D}^T k_3 \tilde{D} \end{aligned} \quad (43)$$

Considering the control law (29), the above Eq. 43 becomes:

$$\dot{V}_2 = -e_1^T \Lambda(e)e_1 - e_1^T \zeta_l - e_2^T k_2 e_2 + e_2^T \tilde{D} + \tilde{D}^T \dot{D} - \tilde{D}^T k_3 \tilde{D} \quad (44)$$

Using equation (22), and considering following inequalities:

$$\begin{aligned} e_2^T \tilde{D} &\leq \frac{e_2^T e_2}{2} + \frac{\tilde{D}^T \tilde{D}}{2} \\ \tilde{D}^T \dot{D} &\leq \frac{\tilde{D}^T \tilde{D}}{2} + \frac{\|\sigma\|^2}{2} \\ e_1^T \zeta_l &\leq \frac{e_1^T e_1}{2} + \frac{\zeta_l^T \zeta_l}{2} \end{aligned} \quad (45)$$

Eq. 44 becomes:

$$\dot{V}_2 \leq -e_1^T \left(\Lambda(e) + \frac{1}{2}I_{7 \times 7} \right) e_1 - e_2^T \left(k_2 - \frac{1}{2}I_{7 \times 7} \right) e_2 - \tilde{D}^T (k_3 - I_{7 \times 7}) \tilde{D} - \frac{\zeta_l^T \zeta_l}{2} + \frac{\|\sigma\|^2}{2} \quad (46)$$

$$\dot{V}_2 \leq -\alpha_1 V_2 + \alpha_2$$

Where, $\alpha_1 = \min\left(\gamma_{\min}\left(\Lambda(e) + \frac{1}{2}I_{7 \times 7}\right), \gamma_{\min}\left(k_2 - \frac{1}{2}I_{7 \times 7}\right), \gamma_{\min}(k_3 - I_{7 \times 7})\right)$ and $\alpha_2 = (1/2)\sigma^2$, under the condition: $k_2 - \frac{1}{2}I_{7 \times 7} > 0$, and $k_3 - I_{7 \times 7} > 0$. Therefore $\dot{V}_2 \leq 0$, whenever $V_2 > \frac{\alpha_2}{\alpha_1}$; which indicates that the rehabilitation robot is stable. Based on Lemma 1 and Eq.46, the variables e_1 , e_2 and \tilde{e}_3 are bounded.

C. Proof of Theorem 2

Consider the following Lyapunov function candidate as:

$$V_3 = V_1 + \frac{1}{2}e_2^T e_2 + \frac{1}{2}\tilde{e}_3^T \tilde{e}_3 \quad (47)$$

where $\tilde{e}_3 = \tilde{D}$. The time derivative of V_3 is given by:

$$\begin{aligned} \dot{V}_3 &= \dot{V}_1 + e_2^T \dot{e}_2 + \tilde{D}^T \dot{\tilde{D}} \\ &= e_1^T (e_2 - \Lambda(e)e_1 - \zeta_l) + e_2^T (U(t) + f(t) + f_{ex}(t) + H(t) - \ddot{\eta}_r) + \tilde{D}^T \dot{D} - \tilde{D}^T k_3 \tilde{D} - \tilde{D}^T k_3 \tilde{H} \end{aligned} \quad (48)$$

Considering the control law (40), \dot{V}_3 can be written as follows:

$$\dot{V}_3 = -e_1^T \Lambda(e)e_1 - e_1^T \zeta_l - e_2^T k_2 e_2 + e_2^T \tilde{H} + e_2^T \tilde{D} + \tilde{D}^T \dot{D} - \tilde{D}^T k_3 \tilde{D} - \tilde{D}^T k_3 \tilde{H} \quad (49)$$

Using Eqs. 22,32, and the following inequalities:

$$\begin{aligned} e_2^T \tilde{D} &\leq \frac{e_2^T e_2}{2} + \frac{\tilde{D}^T \tilde{D}}{2} \\ e_2^T \tilde{H} &\leq \frac{e_2^T e_2}{2} + \frac{|qt_d|^2}{2} \\ \tilde{D}^T \dot{D} &\leq \frac{\tilde{D}^T \tilde{D}}{2} + \frac{\|\sigma\|^2}{2} \\ -\tilde{D}^T k_3 \tilde{H} &\leq \frac{\tilde{D}^T \tilde{D}}{2} + \frac{\|\mathfrak{B}\|^2}{2} \\ e_1^T \zeta_l &\leq \frac{e_1^T e_1}{2} + \frac{\zeta_l^T \zeta_l}{2} \end{aligned} \quad (50)$$

Where $\mathfrak{B} = k_3 qt_d$. Then, Eq. 49 becomes:

$$\begin{aligned} \dot{V}_3 &\leq -e_1^T \left(\Lambda(e) + \frac{1}{2}I_{7 \times 7}\right) e_1 - e_2^T (k_2 - I_{7 \times 7}) e_2 - \tilde{D}^T \left(k_3 - \frac{3}{2}I_{7 \times 7}\right) \tilde{D} - \frac{\zeta_l^T \zeta_l}{2} + \frac{\|\sigma\|^2}{2} + \frac{(qt_d)^2}{2} + \frac{\|\mathfrak{B}\|^2}{2} \\ \dot{V}_3 &\leq -\alpha_1 V_3 + \alpha_2 \end{aligned} \quad (51)$$

Where, $\alpha_1 = \min\left(\gamma_{\min}\left(\Lambda(e) + \frac{1}{2}I_{7 \times 7}\right), \gamma_{\min}(k_2 - I_{7 \times 7}), \gamma_{\min}\left(k_3 - \frac{3}{2}I_{7 \times 7}\right)\right)$, and $\alpha_2 = (1/2)\|\sigma\|^2 + (1/2)(qt_d)^2 + (1/2)\|\mathfrak{B}\|^2$; under the conditions: $k_2 - I_{7 \times 7} > 0$, and $k_3 - \frac{3}{2}I_{7 \times 7} > 0$. This signifies that $\dot{V}_3 \leq 0$, whenever $V_3 > \frac{\alpha_2}{\alpha_1}$; which indicates that the robot system is stable. So, based on Lemma 1 and Eq.51, the variables e_1 , e_2 , \tilde{H} and \tilde{e}_3 are bounded.

REFERENCES

- [1] A.-M. Hughes, S. B. Bouças, J. H. Burridge, M. A. Murphy, J. Buurke, P. Feys, *et al.*, "Evaluation of upper extremity neurorehabilitation using technology: a European Delphi consensus study within the EU COST Action Network on Robotics for Neurorehabilitation," *Journal of neuroengineering and rehabilitation*, vol. 13, p. 86, 2016.
- [2] U. Keller, H. J. van Hedel, V. Klamroth-Marganska, and R. Riener, "ChARMin: The first actuated exoskeleton robot for pediatric arm rehabilitation," *IEEE/ASME Transactions on Mechatronics*, vol. 21, pp. 2201-2213, 2016.
- [3] G. R. Philips, J. J. Daly, and J. C. Príncipe, "Topographical measures of functional connectivity as biomarkers for post-stroke motor recovery," *Journal of NeuroEngineering and Rehabilitation*, vol. 14, p. 67, 2017.

- [4] M. Volpini, V. Bartenbach, M. Pinotti, and R. Riener, "Clinical evaluation of a low-cost robot for use in physiotherapy and gait training," *Journal of Rehabilitation and Assistive Technologies Engineering*, vol. 4, p. 2055668316688410, 2017.
- [5] G. Du and P. Zhang, "A markerless human–robot interface using particle filter and Kalman filter for dual robots," *IEEE Transactions on Industrial Electronics*, vol. 62, pp. 2257-2264, 2015.
- [6] Y. M. Zhao, Y. Lin, F. Xi, and S. Guo, "Calibration-based iterative learning control for path tracking of industrial robots," *IEEE Transactions on industrial electronics*, vol. 62, pp. 2921-2929, 2015.
- [7] J. Ueda, D. Ming, V. Krishnamoorthy, M. Shinohara, and T. Ogasawara, "Individual Muscle Control Using an Exoskeleton Robot for Muscle Function Testing," *IEEE Transactions on Neural Systems and Rehabilitation Engineering*, vol. 18, pp. 339-350, 2010.
- [8] L. Byeong-Kyu, L. Hee-Don, L. Ji-yeong, S. Kyoosik, H. Jung-Soo, and H. Chang-Soo, "Development of dynamic model-based controller for upper limb exoskeleton robot," in *2012 IEEE International Conference on Robotics and Automation*, 2012, pp. 3173-3178.
- [9] M. H. Rahman, M. Saad, J.-P. Kenné, and P. S. Archambault, "Control of an exoskeleton robot arm with sliding mode exponential reaching law," *International Journal of Control, Automation and Systems*, vol. 11, pp. 92-104, 2013.
- [10] K. Kong and M. Tomizuka, "Control of exoskeletons inspired by fictitious gain in human model," *IEEE/ASME Transactions on Mechatronics*, vol. 14, pp. 689-698, 2009.
- [11] G. Hirzinger, N. Sporer, M. Schedl, J. Butterfaß, and M. Grebenstein, "Torque-controlled lightweight arms and articulated hands: Do we reach technological limits now?," *The International Journal of Robotics Research*, vol. 23, pp. 331-340, 2004.
- [12] M. Chen, W. Chen, and Q. Wu, "Adaptive fuzzy tracking control for a class of uncertain MIMO nonlinear systems using disturbance observer," *Science China Information Sciences*, pp. 1-13, 2014.
- [13] H. Tang and Y. Li, "Development and active disturbance rejection control of a compliant micro-/nanopositioning piezostage with dual mode," *IEEE Transactions on Industrial Electronics*, vol. 61, pp. 1475-1492, 2014.
- [14] J. Yang and W. X. Zheng, "Offset-free nonlinear MPC for mismatched disturbance attenuation with application to a static var compensator," *IEEE Transactions on Circuits and Systems II: Express Briefs*, vol. 61, pp. 49-53, 2014.
- [15] E. Sariyildiz and K. Ohnishi, "Stability and robustness of disturbance-observer-based motion control systems," *IEEE Transactions on Industrial Electronics*, vol. 62, pp. 414-422, 2015.
- [16] B. Brahim, S. Maarouf, C. O. Luna, B. Abdelkrim, and M. Rahman, "Adaptive iterative observer based on integral backstepping control for upper extremity exoskeleton robot," in *Modelling, Identification, and Control (ICMIC), 2016 8th International Conference on*, 2016, pp. 886-891.
- [17] C. C. Cheah, "Approximate jacobian control for robot manipulators," in *Advances in Robot Control*, ed: Springer, 2006, pp. 35-53.
- [18] H. Yazarel and C.-C. Cheah, "Task-space adaptive control of robotic manipulators with uncertainties in gravity regressor matrix and kinematics," *IEEE Transactions on Automatic Control*, vol. 47, pp. 1580-1585, 2002.
- [19] A.-C. Huang and M.-C. Chien, *Adaptive control of robot manipulators: a unified regressor-free approach*: World Scientific, 2010.
- [20] A. Brahmī, M. Saad, G. Gauthier, B. Brahmī, W.-H. Zhu, and J. Ghommam, "Adaptive backstepping control of mobile manipulator robot based on virtual decomposition approach," in *Modelling, Identification and Control (ICMIC), 2016 8th International Conference on*, 2016, pp. 707-712.
- [21] W. Chen, S. S. Ge, J. Wu, and M. Gong, "Globally stable adaptive backstepping neural network control for uncertain strict-feedback systems with tracking accuracy known a priori," *IEEE transactions on neural networks and learning systems*, vol. 26, pp. 1842-1854, 2015.
- [22] Z. Li, Z. Huang, W. He, and C.-Y. Su, "Adaptive impedance control for an upper limb robotic exoskeleton using biological signals," *IEEE Transactions on Industrial Electronics*, vol. 64, pp. 1664-1674, 2017.
- [23] Z. Li, C.-Y. Su, G. Li, and H. Su, "Fuzzy approximation-based adaptive backstepping control of an exoskeleton for human upper limbs," *IEEE Transactions on Fuzzy Systems*, vol. 23, pp. 555-566, 2015.
- [24] K. Youcef-Toumi and O. Ito, "A time delay controller for systems with unknown dynamics," in *American Control Conference, 1988*, 1988, pp. 904-913.
- [25] B. Brahmī, M. Saad, C. Ochoa-Luna, and M. H. Rahman, "Adaptive control of an exoskeleton robot with uncertainties on kinematics and dynamics," in *Rehabilitation Robotics (ICORR), 2017 International Conference on*, 2017, pp. 1369-1374.
- [26] M. Jin, J. Lee, and K. K. Ahn, "Continuous nonsingular terminal sliding-mode control of shape memory alloy actuators using time delay estimation," *IEEE/ASME Transactions on Mechatronics*, vol. 20, pp. 899-909, 2015.
- [27] J. Kim, H. Joe, S.-c. Yu, J. S. Lee, and M. Kim, "Time-delay controller design for position control of autonomous underwater vehicle under disturbances," *IEEE Transactions on Industrial Electronics*, vol. 63, pp. 1052-1061, 2016.
- [28] V. Santibañez, K. Camarillo, J. Moreno-Valenzuela, and R. Campa, "A practical PID regulator with bounded torques for robot manipulators," *International Journal of Control, Automation, and Systems*, vol. 8, pp. 544-555, 2010.
- [29] Y. Li, S. Tong, Y. Liu, and T. Li, "Adaptive fuzzy robust output feedback control of nonlinear systems with unknown dead zones based on a small-gain approach," *IEEE Transactions on Fuzzy Systems*, vol. 22, pp. 164-176, 2014.
- [30] L. Zhang, Z. Li, and C. Yang, "Adaptive neural network based variable stiffness control of uncertain robotic systems using disturbance observer," *IEEE Transactions on Industrial Electronics*, vol. 64, pp. 2236-2245, 2017.

- [31] B. Brahmi, M. Saad, J. T. A., T. Lam, C. O. Luna, P. S. Archambault, and M. H. Rahman, "Adaptive control of a 7-DOF exoskeleton robot with uncertainties on kinematics and dynamics," *European Journal of Control*, 2018.
- [32] B. Brahmi, M. Saad, C. Ochoa-Luna, M. H. Rahman, and A. Brahmi, "Adaptive Tracking Control of an Exoskeleton Robot With Uncertain Dynamics Based on Estimated Time-Delay Control," *IEEE/ASME Transactions on Mechatronics*, vol. 23, pp. 575-585, 2018.
- [33] M. H. Rahman, M. J. Rahman, O. Cristobal, M. Saad, J.-P. Kenné, and P. S. Archambault, "Development of a whole arm wearable robotic exoskeleton for rehabilitation and to assist upper limb movements," *Robotica*, vol. 33, pp. 19-39, 2015.
- [34] B. Brahmi, M. Saad, M. H. Rahman, and C. Ochoa-Luna, "Cartesian Trajectory Tracking of a 7-DOF Exoskeleton Robot Based on Human Inverse Kinematics," *IEEE Transactions on Systems, Man, and Cybernetics: Systems*, 2017.
- [35] J. J. Craig, *Introduction to robotics: mechanics and control* vol. 3: Pearson Prentice Hall Upper Saddle River, 2005.
- [36] M. M. Rahman, R. Ikeura, and K. Mizutani, "Investigation of the impedance characteristic of human arm for development of robots to cooperate with humans," *JSME International Journal Series C Mechanical Systems, Machine Elements and Manufacturing*, vol. 45, pp. 510-518, 2002.
- [37] Z. Li, C. Yang, and L. Fan, *Advanced control of wheeled inverted pendulum systems*: Springer Science & Business Media, 2012.
- [38] C. O. Luna, M. H. Rahman, M. Saad, P. Archambault, and W.-H. Zhu, "Virtual decomposition control of an exoskeleton robot arm," *Robotica*, vol. 34, pp. 1587-1609, 2016.